Nanoscale Advances

Accepted Manuscript

This article can be cited before page numbers have been issued, to do this please use: Z. Q. Qiu, P. Zhang, J. Weng, Z. Sun, C. Wang, S. He, J. Lu and J. Hong, *Nanoscale Adv.*, 2026, DOI: 10.1039/D6NA00074F.

ROYAL SOCIETY OF CHEMISTRY

rsc.li/nanoscale-advances

View Article Online
DOI: 10.1039/D6NA00074F

Electric-Field-Driven Magnetic Domain Wall Dynamics: A Multiferroic Route Toward Scalable and Low-Power Spintronic Logic

Peng Zhang[1], Jinghang Weng[1], Zhiyi Sun[1], Chuncheng Wang[1], Shuaitong He[1], Jingjing Lu[1], Zi Qiang Qiu[2], Jeongmin Hong[1,2*]

[1]School of Sciences, Hubei University of Technology, Wuhan, CN

[2]Department of Physics, University of California, Berkeley, CA 94720, USA

*E-mail: jehong@berkeley.edu

Abstract

Magnetic domain walls (DWs) are emerging as promising information carriers in the next generation of high-density, high-speed spintronic devices due to their fast mobility, scalability, and inherent non-volatility. However, conventional DW-based logic architectures rely heavily on external magnetic fields or spin-polarized currents, which hinder large-scale integration due to high energy consumption and limited spatial selectivity. In this study, we present a strain-mediated, electric-field-driven approach to manipulate DWs within multiferroic heterostructures, wherein a ferromagnetic Ni layer is elastically coupled to a piezoelectric PMN-PT substrate. The application of an electric field induces anisotropic strain in the substrate, which is transferred to the ferromagnetic layer, modulating its magnetic anisotropy and enabling deterministic control over DW generation, propagation, and pinning. Through comprehensive micromagnetic simulations, we demonstrate the implementation of fundamental Boolean logic operations through strain-controlled domain-wall motion, illustrating the feasibility of energy-efficient logic-in-memory architectures. Our findings provide a scalable, low-power pathway for next-generation spintronic computing systems using strain-engineered domain-wall logic.

Keywords: Magnetic domain walls, Strain-mediated, Electric-field-driven, Spintronic devices, Logic-in-memory.

View Article Online
DOI: 10.1039/D6NA00074F

1. Introduction

Magnetic domain walls (DWs) have garnered significant interest for their application in spintronic devices such as racetrack memory, logic circuits, and magnetic field sensors.[1-3] These devices offer key advantages—non-volatility, high storage density, fast processing speed, and low energy consumption—that align with the demands of future computing architectures[4-6]. Unlike conventional charge-based electronics, spintronic devices exploit the spin degree of freedom of electrons, enabling persistent memory states without continuous power input.[7] Yet, one of the primary hurdles to the practical deployment of DW-based systems is the precise and energy-efficient control of domain-wall motion within nanowires.[8-9]

In typical spintronic architectures, DWs serve as mobile carriers of binary information. Their generation, movement, and stabilization under external stimuli—such as magnetic fields or spin-polarized currents—are essential for enabling memory and logic functionalities.[10-11] However, these conventional approaches suffer from inherent limitations. Field-driven methods lack spatial selectivity and consume significant power, while current-driven techniques, such as spin-transfer torque (STT), demand high current densities, leading to Joule heating and device degradation.[12-14] Both strategies act globally on the magnetic medium, impeding individual DW control and thus scalability.

To overcome these limitations, we investigate a voltage-driven approach based on strain-mediated magnetoelastic coupling in multiferroic heterostructures.[15-16] In such structures, an electric field applied to a piezoelectric substrate generates a localized strain, which can be elastically transferred to an adjacent ferromagnetic layer. This modulates the magnetic anisotropy of the layer, enabling precise, localized, and energy-efficient control of domain wall behavior.[17-18] By leveraging this coupling, DWs can be generated, steered, and pinned without external magnetic fields or spin currents, dramatically reducing power consumption and enabling fine spatial manipulation.[19-20]

2. Results and discussion

2.1 Device Principle and Material Selection

We present a voltage-controlled multiferroic heterostructure designed for energy-efficient domain wall logic. This platform integrates a ferromagnetic nickel (Ni) thin film deposited on a piezoelectric (011)-oriented PMN-PT substrate. By applying a perpendicular electric field, anisotropic in-plane strain is generated in the PMN-PT layer, which is elastically transferred to the

View Article Online
DOI: 10.1039/D6NA00074F

adjacent Ni film, thereby modulating its magnetic anisotropy. This mechanism enables robust domain formation, propagation, and pinning, offering a foundation for binary switching in logic and memory devices.

The device exploits the tunneling magnetoresistance (TMR) effect to monitor domain evolution. By measuring resistance changes at discrete positions along the nanowire, we achieve real-time tracking of domain wall dynamics. The PMN-PT/Ni interface exhibits strong strain-mediated magnetoelectric coupling, enabling electric-field control of magnetic configurations without the need for spin-polarized currents or external magnetic fields, thereby reducing dissipative current flow and associated Joule heating.

The selection of the PMN-PT/Ni heterostructure was motivated by the requirement for efficient strain-mediated magnetoelectric coupling, balancing material properties and practical applicability. PMN-PT single crystals exhibit exceptionally high piezoelectric coefficients ($d_{33} > 2000$ pC/N) and produce larger electrostrain than conventional PZT ceramics, enabling effective strain generation under moderate electric fields.[21] Although nickel has a lower magnetostriction coefficient ($\lambda_s \approx -33$ ppm) than giant magnetostrictive materials such as Terfenol-D, it offers substantial magnetostriction combined with soft magnetic properties and—critically—excellent compatibility with standard thin-film deposition techniques, including magnetron sputtering and pulsed laser deposition. This compatibility facilitates the integration of continuous, smooth Ni films onto PMN-PT, ensuring strong interfacial strain coupling and efficient magnetization control.

Moreover, the strain-mediated non-volatile modulation of magnetic properties in Ni/PMN-PT has been previously demonstrated, supporting its use in low-energy non-volatile logic devices.[22] Although many strain-mediated multiferroic systems have been explored to maximize magnetoelectric coefficients, often motivated by sensing-oriented applications, the PMN-PT/Ni configuration provides an optimal balance between magnetoelectric coupling strength, experimental reproducibility, and material stability. This combination is particularly suitable for systematic studies of domain wall dynamics in a well-defined system for logic operations.

The non-volatile retention of strain in our device originates from the ferroelastic domain switching in the (011)-oriented PMN-PT substrate. PMN-PT exhibits a rhombohedral crystal structure at room temperature, with spontaneous polarization vectors oriented along the <111> family of directions. When an out-of-plane electric field is applied, the polarization can reorient among these

View Article Online
DOI: 10.1039/D6NA00074F

equivalent <111> directions predominantly via non-180° ferroelastic switching (e.g., 71° or 109° rotations), rather than purely 180° reversal. This ferroelastic reorientation is accompanied by a lattice distortion that generates a pronounced anisotropic in-plane strain. Importantly, the strain-electric-field response is hysteretic, so the ferroelectric/ferroelastic domains can remain in a switched metastable state after the electric field is removed and produce a non-zero remanent strain. Through elastic coupling, this remanent strain is transferred to the adjacent Ni film and imprints a non-volatile modulation of magnetic anisotropy, enabling the magnetic state to be retained without continuous power input.

Figs. 1a and 1b depict the anisotropic piezoelectric strain response of the PMN-PT substrate under a vertical electric field applied along the [011] direction. Upon application of an upward electric field (+*E*), the substrate manifests a tensile strain along the in-plane [01$\bar{1}$] axis and a concurrent compressive strain along the [100] axis. Conversely, reversing the field direction to downward (-*E*) induces a complete switching of the strain polarities in both directions. This deterministic strain modulation is instrumental for the reconfigurable control of magnetic domain structures and magnetization dynamics within the adjacent ferromagnetic layer, serving as the physical building block for strain-mediated logic and memory functionalities.

Structural characterization via microscopy confirms the smooth surface morphology of the Ni films deposited on both PMN-PT and SiO_2 substrates, as shown in Figs. 1c and 1d. The uniform and continuous film morphology supports efficient elastic strain transfer at the PMN-PT/Ni interface and helps minimize extrinsic pinning associated with surface inhomogeneity, providing a reliable materials platform for strain-mediated control of magnetic anisotropy and domain-wall behavior. Our proposed logic device is based on a well-established multiferroic heterostructure consisting of a ferromagnetic nickel (Ni) thin film elastically coupled to a piezoelectric (011)-oriented PMN-PT substrate.[23] This material system has been extensively studied and exhibits strong strain-mediated magnetoelectric coupling at room temperature. Notably, the (011)-oriented PMN-PT exhibits non-180° ferroelastic switching, which generates a non-volatile, anisotropic in-plane strain upon application and subsequent removal of an electric field.[24] The resulting remanent strain is transferred to the Ni layer and imprints a non-volatile modulation of magnetic anisotropy, which forms the basis for the voltage-controlled DW operations discussed below.

View Article Online
DOI: 10.1039/D6NA00074F

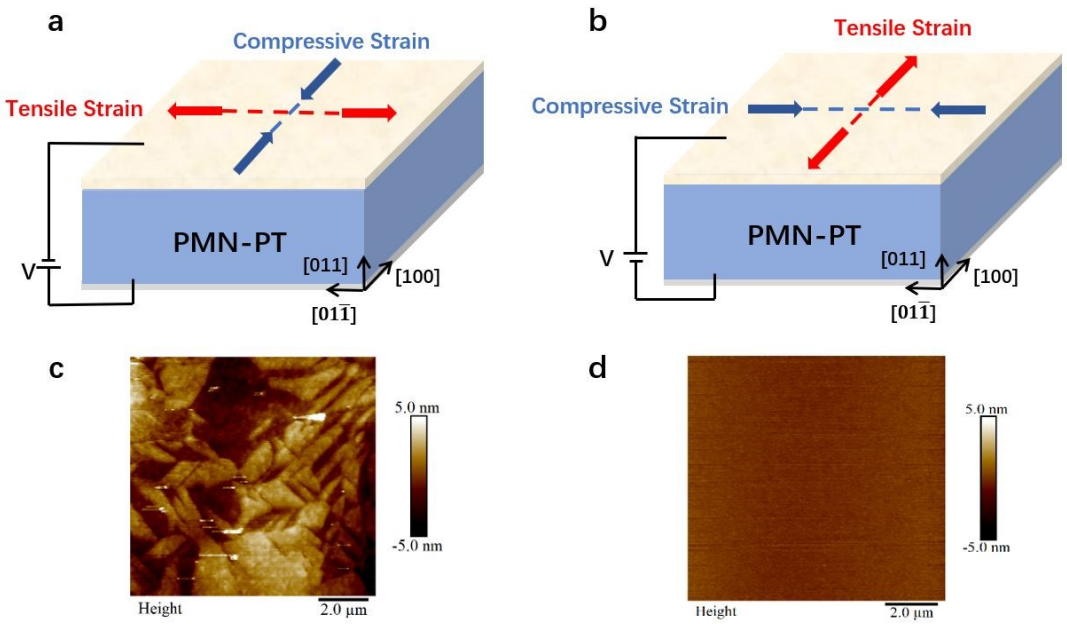

Fig. 1 Principle and structure of strain-mediated magnetoelastic coupling of PMN-PT/Ni heterostructures. (a and b) Schematic illustration of anisotropic in-plane strain generated in (011)-oriented PMN-PT under out-of-plane electric fields with opposite polarities. The strain state switches between compressive and tensile components along the orthogonal in-plane crystallographic axes. (c and d) Atomic force microscopy (AFM) images showing the surface morphology of Ni thin films deposited on PMN-PT and SiO_2 substrates, respectively, confirming a continuous and smooth film suitable for efficient elastic strain transfer.

The configuration consists of a nickel (Ni) thin film exhibiting in-plane magnetic anisotropy deposited onto a single-crystal PMN-PT substrate with a (011) orientation. Nickel electrodes are positioned at both ends of the nanowire, leaving a central electrode-free region to define a localized strain-gradient profile under an applied electric field. This architecture enables strain-mediated control of magnetization within the active region.

To quantitatively investigate the strain-mediated domain-wall dynamics in the PMN-PT/Ni heterostructure, we performed coupled finite-element and micromagnetic simulations using COMSOL Multiphysics and the Object-Oriented Micromagnetic Framework. The simulation workflow consisted of two sequential stages: (1) calculation of the electric-field-induced strain distribution in the multiferroic heterostructure using COMSOL, and (2) simulation of magnetization dynamics under the computed strain field using OOMMF.

In COMSOL, the piezoelectric substrate was modeled using the Piezoelectric Devices module with material parameters for (011)-oriented PMN-PT single crystals: relative permittivity tensor ε_r =

View Article Online
DOI: 10.1039/D6NA00074F

diag(4235, 1081, 3873), and piezoelectric coefficient matrix d_{ij} with dominant components d_{33} = 58.481 pC/N, d_{31} = 32.4432 pC/N, d_{15} = 10.72 pC/N. The Ni thin film was defined as an isotropic linear elastic material (Young's modulus Y = 214 GPa, Poisson's ratio ν = 0.31).[25] A static electric potential (±400 V) was applied across the substrate thickness (500 μm), and the resulting mechanical displacement field at the PMN-PT/Ni interface was exported and interpolated onto a uniform 5-nm grid.

The displacement field was then converted into a strain tensor field ε_{ij} and imported into OOMMF via a custom magnetoelastic extension module based on the standard magnetoelastic energy formalism. Perfect elastic strain transfer from PMN-PT to the Ni layer was assumed. Within OOMMF, the Ni nanowire was discretized into cuboidal cells of size 5×5×1 nm^3, smaller than the exchange length of Ni ($l_{ex} \approx 7.6$ nm). The magnetic energy functional included exchange, Zeeman, demagnetization, an effective uniaxial anisotropy (K_u = 1×10^4 J/m^3, easy axis along [01$\bar{1}$]), and magnetoelastic contributions. The magnetoelastic energy density was implemented as:[26]

$$E_{me}=B_1(m_x^2\varepsilon_{xx}+m_y^2\varepsilon_{yy}+m_z^2\varepsilon_{zz})+B_2(m_xm_y\varepsilon_{xy}+m_xm_z\varepsilon_{xz}+m_ym_z\varepsilon_{yz}) \quad (1)$$

where $\mathbf{m} = (m_x, m_y, m_z) = \mathbf{M}/M_s$ is the normalized magnetization vector, M_s = 6.6×10^5 A/m, and the magnetoelastic coupling coefficients B_1 = -6.2×10^6 J/m^3 and B_2 = -9.0×10^6 J/m^3 were derived from the saturation magnetostriction constant of Ni ($\lambda_s \approx$ -33.9×10^{-6}) and its elastic constants. This formulation directly incorporates the full strain tensor into the effective magnetic field:

$$\mathbf{H}_{me}=-\frac{1}{\mu_0 M_s}\frac{\partial E_{me}}{\partial \mathbf{m}} \quad (2)$$

which is then included in the Landau-Lifshitz-Gilbert (LLG) equation:

$$\frac{\partial \mathbf{m}}{\partial t}=-\gamma \mathbf{m}\times\mathbf{H}_{eff}+\alpha \mathbf{m}\times\frac{\partial \mathbf{m}}{\partial t} \quad (3)$$

thereby modulating the local magnetic anisotropy in a spatially varying manner. The Landau-Lifshitz-Gilbert equation was solved with a damping constant α = 0.045 to simulate the time evolution of magnetization under applied voltage sequences.

To initialize the system, the left Ni electrode was grounded while a +400 V potential was applied to the bottom of the PMN-PT substrate, thereby generating a vertical electric field of approximately 8 kV/cm. Through converse piezoelectric coupling, this electric field induces a mechanical strain distribution in the (011)-oriented PMN-PT substrate, characterized by compressive strain along [100] and tensile strain along [01$\bar{1}$], as shown in Figs. 2a and 2c. To further quantify the non-uniform strain profile, Fig. 2d plots the extracted ε_{xx} line profile along the dashed path in Fig. 2c,

View Article Online
DOI: 10.1039/D6NA00074F

highlighting the spatial decay of strain away from the electrode edge and the resulting strain gradient.

Specifically, prior in situ X-ray diffraction studies have shown that PMN-PT single crystals can generate a pronounced electric-field-induced anisotropic lattice strain, with the strain response strongly dependent on crystal orientation and ferroelastic domain switching pathways. Consistent with these reports, our simulations predict an anisotropic in-plane strain of approximately -0.12% along [100] and +0.15% along $[0\bar{1}1]$ under an applied field of ~8 kV/cm. These strain magnitudes fall within the range commonly reported for PMN-PT under comparable electric-field conditions.[27]

The deterministic control of magnetic DWs in our multiferroic heterostructure is fundamentally governed by the electric-field-induced modulation of magnetic anisotropy via magnetoelastic coupling. To quantitatively assess this effect, we calculate the change in magnetic anisotropy energy density K_{me}, resulting from the piezoelectric strain transferred to the Ni film. For a cubic ferromagnet like Ni, the magnetoelastic contribution to the anisotropy energy density along a given direction is given by:

$$K_{me} = \frac{3}{2}\lambda_s Y \varepsilon_{eff} \quad (4)$$

where $\lambda_s \approx -33.9\times10^{-6}$ is the saturation magnetostriction coefficient of Ni (negative sign indicates that the magnetization prefers to align perpendicular to the direction of tensile strain), Y = 214 GPa is its Young's modulus, and ε_{eff} is the effective in-plane strain component along the magnetization direction. $\varepsilon_{eff} \approx 0.1\%$ represents the effective anisotropic strain transferred from the PMN-PT substrate, a value consistent with the typical non-linear ferroelastic strain output of (011)-oriented PMN-PT single crystals near the coercive field. Substituting these physical parameters into the equation yields a strain-induced anisotropy magnitude of $|K_{me}| \approx 1.0\times10^4$ J/m^3. Owing to $\lambda_s < 0$, tensile strain makes the strained axis magnetically unfavorable, so the effective easy axis is expected to rotate perpendicular to the tensile direction. This strain-imprinted anisotropy is comparable to or larger than the intrinsic anisotropy terms of the Ni film, and therefore provides a strong driving force for the observed domain wall dynamics.

2.2 Mechanism of Strain-Induced Domain Wall Generation and Propagation

The 400 V potential applied across the 500 μm-thick PMN-PT substrate generates an electric field of 8 kV/cm, which serves as the fundamental driving parameter for strain induction. This field strength represents a well-established operational regime for bulk ferroelectric materials that

View Article Online
DOI: 10.1039/D6NA00074F

ensures reliable and reversible ferroelastic switching while remaining below typical dielectric breakdown thresholds. The relatively high voltage magnitude is principally determined by the substrate thickness ($V = E \cdot d$) rather than the field strength requirement itself, reflecting our use of a commercially available macroscopic substrate in the present device geometry.

Micromagnetic simulations conducted using OOMMF reveal that the applied voltage sequence produces distinct domain-wall responses through strain-mediated anisotropy modulation. An initial +8 kV/cm pulse generates an anisotropic in-plane strain statecompressive strain along [100] and tensile strain along [01$\bar{1}$], imprinting a localized magnetoelastic anisotropy gradient that drives partial (~90°) magnetization rotation near the left electrode (Fig. 2b). Reversing the field to -8 kV/cm switches the strain state, enabling the nucleation of a reversed domain and subsequent unidirectional domain-wall propagation toward the right electrode (Fig. 2e). As the strain-induced anisotropy gradient decays away from the electrode region, the driving force is reduced and DW becomes pinned near the nanowire end. This polarity-dependent behavior is enabled by the hysteretic ferroelastic response of the PMN-PT substrate, which gives rise to a butterfly-shaped strain-electric-field loop and remanent anisotropic strain after field removal.[28] In our model, the remanent strain is assumed to persist between pulses and thus provides a non-volatile magnetoelastic energy landscape in the adjacent Ni layer. Furthermore, applying voltages simultaneously to both electrodes produces a more uniform strain profile in the central region, enabling intentional DW pinning between electrodes and demonstrating spatially programmable DW manipulation without global current flow.

The contrasting domain-wall dynamics under opposite electric-field polarities originate from the sign reversal of the induced in-plane strain tensor combined with the negative magnetostriction of Ni (($\lambda_s < 0$). In particular, reversing the electric-field polarity switches the orientation of the magnetoelastic easy axis relative to the nanowire shape-anisotropy axis, which favors either local magnetization rotation and domain-wall nucleation (“driving” condition) or the stabilization of antiparallel domains leading to a 180° Néel-type domain wall (“holding” condition).

View Article Online
DOI: 10.1039/D6NA00074F

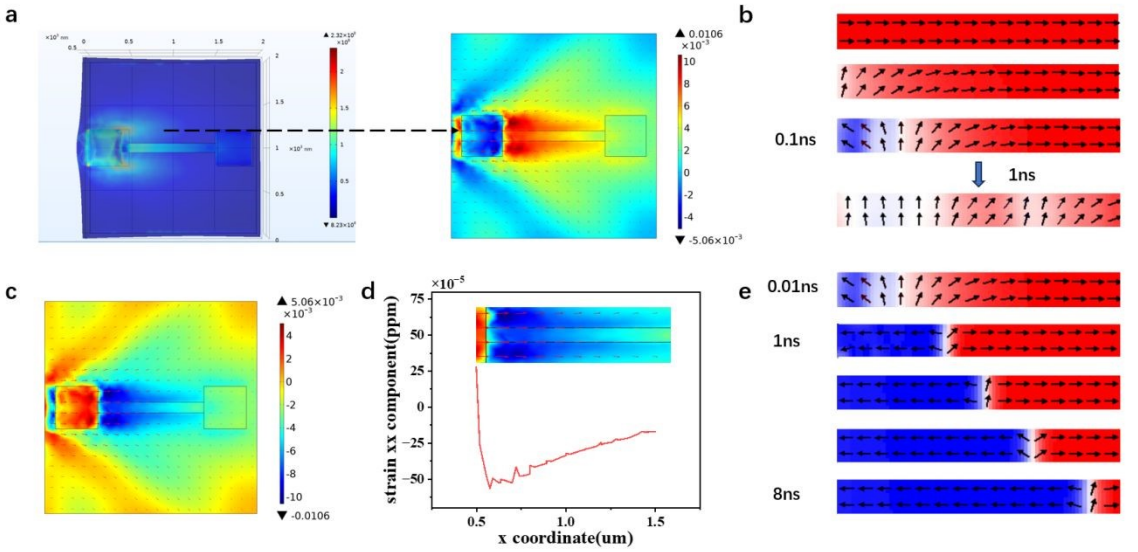

Fig. 2 Voltage-induced strain distribution and domain-wall dynamics in the PMN-PT/Ni heterostructure. (a and c) COMSOL-simulated in-plane strain distribution in the Ni nanowire under out-of-plane electric fields of +8 kV/cm and -8 kV/cm. (d) Line profile of ε_{xx} extracted along the dashed path in (c), highlighting the strain gradient that provides the driving force for subsequent domain-wall motion. (b and e) OOMMF snapshots of magnetization evolution under +8 kV/cm and -8 kV/cm, demonstrating polarity-dependent domain-wall nucleation and propagation.

2.3 Domain Wall Velocity and Micromagnetic Optimization

The velocity of magnetic DWs is a key performance metric for domain-wall-based spintronic logic, as it directly impacts switching speed and computational throughput. To optimize the propagation speed and stability of DW motion, we systematically varied the nanowire geometry and electrode configuration in micromagnetic simulations. The simulations incorporated realistic stress distributions and boundary conditions derived from COMSOL-generated strain profiles.

Simulation results indicate that the nanowire geometry and electrode configuration can influence the propagation behavior and stability of domain-wall motion. In particular, the nanowire length and width, together with the electrode layout, were treated as key design parameters in our optimization study. Fig. 3a schematically illustrates the device geometry and the geometric parameters used to parameterize the simulations, where *A*, *B*, and *C* represent the Ni electrode size, nanowire length, and nanowire width, respectively.

Furthermore, domain-wall dynamics depend on the intrinsic exchange stiffness of the ferromagnetic layer, which governs the domain-wall width and internal rigidity. In our simulations,

View Article Online
DOI: 10.1039/D6NA00074F

we used the standard exchange stiffness of Ni (15×10^{-12} J/m). The resulting domain-wall mobility is therefore governed mainly by the voltage-induced magnetoelastic anisotropy gradient and geometric confinement, indicating that device-level optimization can be achieved without modifying intrinsic exchange properties.

Fig. 3b summarizes the simulated DW propagation velocity for different geometric parameter sets, while Figs. 3c and 3d present the final magnetization configurations for nanowires with varying lengths and widths, respectively. The results identify optimal design for maximizing DW velocity, corresponding to a Ni electrode size of 400 nm (*A*), a nanowire length of 400 nm (*B*), and a nanowire width of 50 nm (*C*). Under these conditions, the simulated DW reaches a peak velocity of approximately 266 m/s, indicating efficient voltage-driven propulsion in the strain-mediated multiferroic heterostructure. This geometric ratio optimizes the strain gradient distribution transmitted from the PMN-PT substrate to the Ni nanowire. In particular, matching the electrode size with the nanowire length helps confine the effective strain-gradient region within the active segment and improves the directional consistency of the strain-induced driving landscape, thereby mitigating strain dispersion caused by geometric mismatch. In addition, a relatively narrow nanowire width (e.g., ~50 nm in our optimized design) enhances lateral mechanical confinement and strengthens the magnetoelastic anisotropy gradient, which lowers the effective energy barrier for domain-wall motion and improving the driving efficiency. The attained DW velocity is on the order of 10^2 m/s (with a peak value of ~266 m/s). This indicates efficient strain-mediated propulsion under voltage control. Within the explored driving range, we do not observe pronounced signatures of Walker-type breakdown, such as precessional instability or periodic transformations of the wall structure. This can be attributed to the spatially graded magnetoelastic anisotropy, which provides a non-uniform driving landscape and helps maintain stable DW propagation compared with uniformly driven nanowires. Under this mechanism, the maximum attainable velocity is expected to be primarily limited by the magnitude and spatial extent of the engineered strain-induced anisotropy gradient, rather than by intrinsic dynamic instabilities of the DW itself. These results highlight the feasibility of strain-engineered DW devices for fast and energy-efficient logic and memory operations.

View Article Online
DOI: 10.1039/D6NA00074F

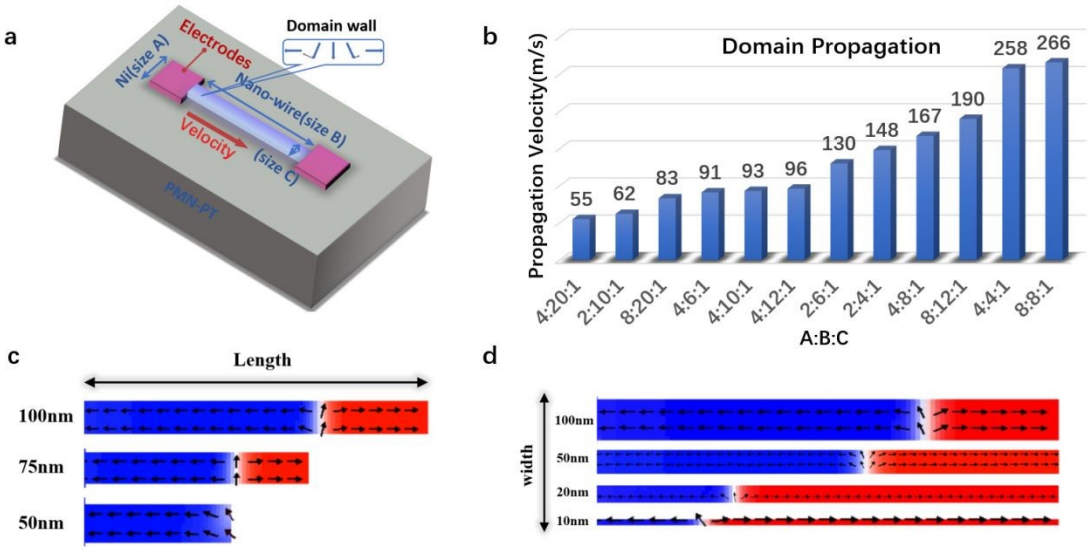

Fig. 3 Magnetic domain-wall propagation velocity. (a) Schematic of the device geometry used for micromagnetic optimization, where *A* denotes the Ni electrode size, *B* the Ni nanowire length, and *C* the Ni nanowire width. (b) Domain-wall propagation velocity for different *A*:*B*:*C* ratios. (c) Final magnetization configurations after voltage actuation for nanowires with different lengths *B*. (d) Final magnetization configurations after voltage actuation for nanowires with different widths *C*.

2.4 Energy Consumption Analysis

The energy efficiency of strain-mediated domain-wall control is a key advantage over conventional spintronic techniques. In the PMN-PT/Ni heterostructure, the energy cost per operation is mainly determined by the voltage-driven charging of the ferroelectric/piezoelectric layer, rather than by Joule heating associated with large current densities in current-driven devices.

The total energy consumed during one voltage-controlled actuation event can be approximated as

$$E_{total} = \frac{1}{2}\varepsilon_0\varepsilon_r\frac{A}{d}V^2 + P_r A E_c d + k_B T \ln 2 \quad (5)$$

where the first term represents the capacitive charging energy of the PMN-PT substrate treated as a parallel-plate capacitor ($C = \varepsilon_0\varepsilon_r A/d$). Here, A denotes the electrode area, d is the substrate thickness, ε_r is the relative permittivity, and V is the applied voltage. The second term corresponds to the energy associated with ferroelectric polarization switching, parameterized by the remnant polarization P_r and coercive field E_c. The third term, $k_B T \ln 2$, is the Landauer limit, which provides the theoretical minimum energy for an irreversible bit operation at temperature T and is included here as a benchmark for comparison.[29]

Using representative material parameters and device dimensions, the total energy consumption is estimated to be 284.5 fJ per operation. The capacitive contribution dominates (283 fJ, ~99.5% of

View Article Online
DOI: 10.1039/D6NA00074F

the total), while the polarization switching term contributes ~1.5 fJ (~0.5%). In contrast, the Landauer limit is ~2.87 aJ, which is negligible on this energy scale.

Furthermore, the non-volatile nature of the strain-induced magnetic anisotropy originates from the ferroelastic hysteresis of the (011)-oriented PMN-PT substrate, which can retain a remanent strain state after voltage removal. This allows the magnetic configuration to persist without continuous power input, thereby reducing static power dissipation during memory retention and standby operation. Overall, our analysis indicates that electric-field-controlled domain-wall propagation in multiferroic systems can combine high spatial selectivity with low switching energy, offering a promising route toward low-power spintronic logic and memory devices.

2.5 Logic Gate Structures and Operation

To demonstrate the application of electric-field-driven domain-wall motion in logic computation, we propose and simulate two multiferroic logic gate architectures, one implementing AND/NAND operations and the other enabling OR/NOR functionality (Fig. 4a,d). Each device consists of a ferromagnetic Ni nanowire elastically coupled to an (011)-oriented PMN-PT substrate, with two independently addressable top electrodes serving as logic inputs.

Logic input A corresponds to the left electrode and logic input B to the right electrode. In our encoding scheme, an applied voltage pulse (400 V) represents logic state ‘1’ by generating a local strain field, whereas a grounded electrode represents logic state ‘0’. In the initial AB = 00 configuration, no voltage is applied to either input electrode, and the nanowire remains in its initial magnetic state with no additional strain-driven actuation. When AB = 10 or AB = 01, a voltage applied to a single electrode generates a localized strain field near the activated input, which modifies the local magnetoelastic anisotropy and triggers a corresponding domain reconfiguration and domain-wall motion along the nanowire. In the AB = 11 case, simultaneous activation of both electrodes produces a combined strain landscape, resulting in a distinct domain configuration and output state.

Micromagnetic simulations capture the domain-wall responses under all four input combinations, and the corresponding magnetization configurations are shown in Figs. 4b and 4e. These results confirm that the proposed structures can implement the targeted Boolean logic functions through strain-mediated domain reconfiguration and domain-wall displacement.

View Article Online
DOI: 10.1039/D6NA00074F

To read the output, a magnetic tunnel junction (MTJ) is placed on top of the nanowire as a TMR-based sensing element, where the fixed reference layer is provided by the MTJ and the local magnetization of the underlying nanowire serves as the effective free layer. The resistance state is determined by the relative magnetization alignment between the reference layer and the underlying magnetic domain. Here, we define the low-resistance (parallel) state as logic "0" and the high-resistance (antiparallel) state as logic "1", enabling non-volatile electrical readout of the logic output. Furthermore, logic reconfigurability can be achieved by adjusting the MTJ position along the nanowire and reversing the magnetization direction of the reference layer. With this configuration, the same device layout can implement different Boolean operations without hardware modification. The corresponding truth tables and magnetic configurations are summarized in Figs. 4c and 4f.

The strain-mediated electric-field control of magnetic DWs in multiferroic Ni/PMN-PT heterostructures presents several key advancements over existing approaches, particularly in the implementation of AND/NAND logic gates. Unlike the XOR/XNOR and OR/NAND architectures demonstrated in prior work, which rely on fixed structural configurations to define logic functionality, our platform introduces dynamic reconfigurability as a core innovation.[30] By adjusting the placement of MTJs and the magnetization direction of the reference layer, the same physical device can switch between AND, NAND, OR, and NOR operations without hardware modifications. These results underscore the feasibility of implementing fundamental Boolean logic operations using strain-driven domain-wall motion. Compared with current-driven schemes, the proposed strain-mediated approach can potentially improve energy efficiency and mitigate Joule-heating-related scaling constraints, offering a promising route toward next-generation non-volatile logic computing.

An important implication of the proposed strain-mediated domain-wall scheme is its potential compatibility with pulse-driven, sequential logic operation. In our device geometry, a voltage pulse applied to a local electrode generates a transient, spatially nonuniform strain distribution, which can be used to temporally gate domain-wall nucleation and propagation. Because both the ferroelastic strain state in PMN-PT and the strain-imprinted magnetic configuration in Ni can exhibit remanence, intermediate magnetic states may be retained after the voltage is removed, suggesting an intrinsic state-holding capability without continuous power consumption. In addition, the spatial decay of the strain field can introduce an effective directionality to the domain-wall

View Article Online
DOI: 10.1039/D6NA00074F

response, which may be beneficial for staged signal transfer in multielectrode designs. These features motivate the exploration of multistage, pulse-sequenced architectures in future work.

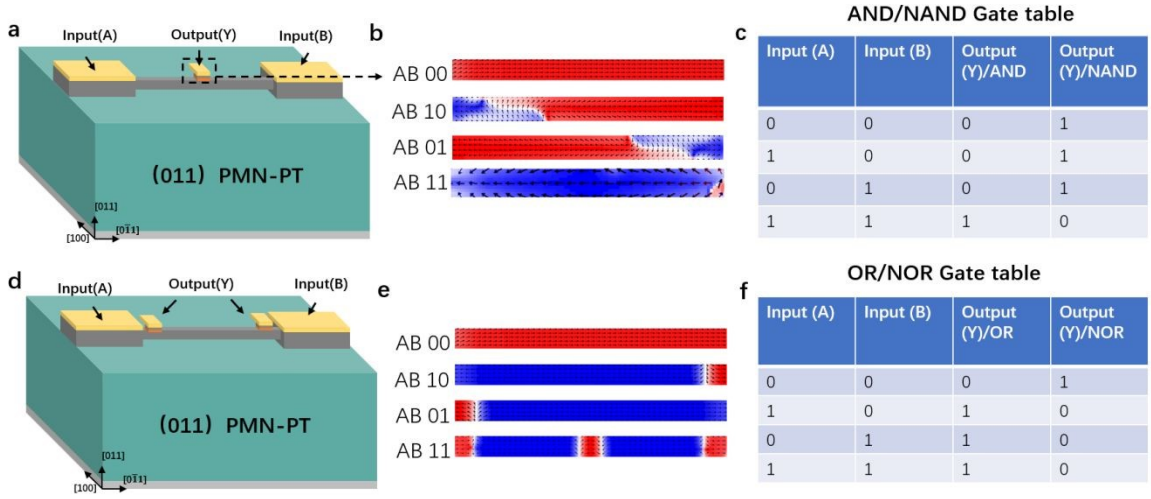

Input (A)	Input (B)	Output (Y)/AND	Output (Y)/NAND
0	0	0	1
1	0	0	1
0	1	0	1
1	1	1	0

Input (A)	Input (B)	Output (Y)/OR	Output (Y)/NOR
0	0	0	1
1	0	1	0
0	1	1	0
1	1	1	0

Fig. 4 Implementation of multiferroic heterostructure logic devices based on strain-mediated domain-wall motion. (a) Schematic of the AND/NAND logic-gate structure with two input electrodes (A and B) and the output readout position (Y). (b) Simulated magnetization configurations for the AND/NAND gate under the four input combinations (AB = 00, 10, 01, and 11). (c) Corresponding truth table and output states for AND and NAND operations. (d) Schematic of the OR/NOR logic-gate structure. (e) Simulated magnetization configurations for the OR/NOR gate under the four input combinations (AB = 00, 10, 01, and 11). (f) Corresponding truth table and output states for OR and NOR operations.

2.6 Considerations for Device Reliability and Scalability

The practical deployment of nanoscale spintronic devices requires consideration of effects that can influence operational reliability. Here, we discuss the implications of thermal fluctuations and fabrication imperfections, such as edge roughness, on the performance of our strain-mediated domain-wall logic.

To evaluate the robustness of the retained states against thermal agitation, we estimate the thermal stability by comparing the strain-induced pinning barrier ΔE with the room-temperature (300 K) thermal energy $k_B T$ (~4.1×10^{-21} J). In our architecture, the magnetic domain wall (DW) is pinned by a localized energy minimum in the strain-imprinted anisotropy landscape. The depinning energy barrier can be expressed as $\Delta E \approx K_{\mathrm{eff}} \times V_{\mathrm{DW}}$.

For a Néel-type wall in our Ni nanowire (width w = 50 nm, thickness t = 10 nm), the DW width δ is governed by the effective anisotropy energy density K_{eff} which arises from the superposition of the strain-mediated magnetoelastic anisotropy K_{me} and the shape anisotropy K_{shape} intrinsic to the

View Article Online
DOI: 10.1039/D6NA00074F

nanowire's geometry. With $|K_{me}| \approx 1.0\times10^4$ J/m^3, K_{shape} is calculated as:

$$K_{shape} \approx \frac{1}{2}\mu_0 M_s{}^2\left(\frac{t}{w}\right) \quad (6)$$

where μ_0 is the vacuum permeability and $Ms = 6.6\times10^5$ A/m is the saturation magnetization of Ni. Substituting the geometry yields $K_{shape} \approx 5.5\times10^4$ J/m^3, resulting in a total $K_{eff} = |K_{me}| + K_{shape} \approx 6.5\times10^4$ J/m^3. The exchange-stiffness-dominated DW width is therefore

$$\delta = \pi\sqrt{A/|K_{me}|} \quad (7)$$

where $A = 15$ pJ/m is the exchange stiffness constant of Ni. This gives $\delta \approx 27$ nm. The effective volume of the DW core is $V_{DW} \approx w \times t \times \delta \approx 1.35\times10^{-23}$ m^3. Consequently, the pinning energy barrier is estimated as $\Delta E \approx K_{eff} \times V_{DW} \approx 8.8\times10^{-19}$ J. The derived thermal stability factor, $\Delta E/k_BT \approx 215$, exceeds the empirical threshold of 40 required for long-term non-volatile data retention. This confirms that the strain-mediated pinning mechanism in our device establishes a thermally robust energy barrier, effectively stabilizing the magnetic logic states against random thermal fluctuations at room temperature.

Nanowire edge roughness, arising from fabrication limitations, can introduce local variations in shape anisotropy and create unintended pinning sites that interfere with deterministic domain-wall motion. As discussed by Misba *et al.*[31], edge roughness can lead to stochastic depinning, velocity dispersion, and device-to-device variability in DW-based devices. In our strain-mediated approach, the driving force is provided by a distributed strain gradient acting over the domain-wall profile, which is expected to be less sensitive to atomic-scale edge defects than torques concentrated at specific regions. Nevertheless, pronounced roughness can still perturb the local magnetization and modify the effective potential landscape. Future experimental implementations would therefore benefit from advanced lithography and etching processes to minimize sidewall roughness, thereby improving reproducibility of domain-wall propagation.

3. Advantages and Future Prospects

Strain-mediated manipulation of magnetic DWs in multiferroic heterostructures provides a voltage-controlled route for domain-wall-based logic, offering an alternative to conventional field- or current-driven actuation schemes. By utilizing electric-field-induced strain to modulate magnetic anisotropy through magnetoelastic coupling, the approach enables localized control of DW nucleation, propagation, and pinning without requiring a continuous charge current through the ferromagnetic channel.

View Article Online
DOI: 10.1039/D6NA00074F

While domain-wall motion serves as the foundational principle shared with racetrack memory architectures, such as those proposed by Hayashi et al.[32] and Roy et al.[33], our strain-mediated approach introduces three key innovations that broaden its application scope. First, the actuation mechanism replaces current-driven spin-transfer torque (STT), which typically requires current densities on the order of 10^7 A/cm^2 and is associated with Joule heating and scalability limitations, with localized electric-field-induced strain coupling.[34] This shift largely avoids ohmic losses in the magnetic channel and enables sub-micron spatial selectivity that is difficult to achieve using global current injection alone.

Second, the device architecture utilizes engineered strain gradients (typically within submicron length scales) across multiferroic heterostructures to create localized logic gates. This differs from racetrack designs that employ serial nanowires primarily for sequential data shifting. In comparison, our approach facilitates spatially localized logic operations within compact footprints, which is favorable for parallel integration of multiple logic gates.

Third, our functionality extends beyond the "shift-register" paradigm characteristic of racetrack systems. By integrating voltage-controlled strain profiles with reconfigurable MTJs, our platform enables Boolean logic operations (AND/NAND/OR/NOR) with programmable readout. Unlike the fixed data-shuttling paths in traditional racetracks, the logic functions can be switched by adjusting MTJ placement or reference-layer magnetization, allowing hardware-level reconfigurability without physical redesigns. This "logic-in-memory" capability, combined with field-free operation and non-volatility, highlights strain-mediated domain-wall logic for energy-efficient computing beyond conventional memory applications.

Collectively, these characteristics suggest that strain-mediated DW logic can provide a scalable route toward compact, field-free, and reconfigurable spintronic logic, motivating further studies on device integration and performance optimization. Multiferroic platforms can facilitate device miniaturization and high-density integration by enabling voltage-controlled actuation in compact heterostructures, which is compatible with scalable thin-film fabrication processes. By tuning the placement of MTJs and the polarity of the applied voltages, the same physical structure can be configured to implement different logic functions (AND, NAND, OR, and NOR) without modifying the nanowire geometry. In addition, field-free operation eliminates the need for

View Article Online
DOI: 10.1039/D6NA00074F

externally applied magnetic fields, which simplifies circuit integration and reduces operational constraints associated with field-driven switching schemes.

Future research directions include further scaling of device dimensions, improving switching speed through optimized strain profiles and electrode designs, and exploring integration with CMOS-compatible process flows. Beyond Boolean logic, strain-controlled domain-wall configurations may also be of interest for non-conventional computing paradigms such as neuromorphic or analog-inspired functionalities, although dedicated device designs and systematic validation are required.

4. Conclusion

In this work, we introduce an electric-field-driven mechanism for domain-wall (DW) manipulation in multiferroic Ni/PMN-PT heterostructures and demonstrate its potential for low-power, reconfigurable spintronic logic. By leveraging strain-mediated magnetoelectric coupling, voltage pulses can induce controlled DW generation, propagation, and pinning without external magnetic fields or current-driven spin torques. Micromagnetic simulations, supported by structural characterization of the heterostructure, confirm the feasibility of implementing Boolean logic gates, including AND/NAND and OR/NOR, using programmable strain fields. The DW motion is governed by the applied voltage polarity, and the output state can be read through tunneling magnetoresistance, providing a practical route toward logic-in-memory operation. Overall, this strain-mediated DW platform combines localized voltage control, non-volatile state retention, and reconfigurable logic functionality, and may offer a promising direction for future non-volatile spintronic computing.

View Article Online
DOI: 10.1039/D6NA00074F

References

1. D. Kumar, T. Jin, S. Al Risi, R. Sbiaa, W. S. Lew and S. N. Piramanayagam, *IEEE Trans. Magn.*, 2019, **55(3)**, 1–8.
2. J. Wang, J. Ma, H. Huang, J. Ma, H. M. Jafri, Y. Fan, H. Yang, Y. Wang, M. Chen, D. Liu, J. Zhang, Y.-H. Lin, L.-Q. Chen, D. Yi and C.-W. Nan, *Nat. Commun.*, 2022, **13**, 3255.
3. G. Venkat, D. A. Allwood and T. J. Hayward, *J. Phys. D: Appl. Phys.*, 2024, **57**, 063001.
4. S. Umesh and S. Mittal, *Journal of Systems Architecture*, 2019, **97**, 349–372.
5. K. Wagner, A. Kákay, K. Schultheiss, A. Henschke, T. Sebastian and H. Schultheiss, *Nat. Nanotechnol.*, 2016, **11**, 432–436.
6. A. Roohi, R. Zand and R. F. DeMara, *IEEE Trans. Magn*., 2016, **52(8)**, 1–7.
7. P. Barla, V. K. Joshi and S. Bhat, *J. Comput. Electron*, 2021, **20**, 805–837.
8. P. Sethi, S. Krishnia, W. L. Gan, F. N. Kholid, F. N. Tan, R. Maddu and W. S. Lew, *Sci. Rep.*, 2017, **7**, 4964.
9. M. Wu, T. Chen, T. Nomoto, Y. Tserkovnyak, H. Isshiki, Y. Nakatani, T. Higo, T. Tomita, K. Kondou, R. Arita, S. Nakatsuji and Y. Otani, *Nat. Commun.*, 2024, **15**, 4305.
10. C. A. Durner, A. Migliorini, J.-C. Jeon and S. S. P. Parkin, *ACS Nano*, 2025, **19**, 5316–5325.
11. J.-C. Jeon, A. Migliorini, L. Fischer, J. Yoon and S. S. P. Parkin, *ACS Nano*, 2024, **18**, 14507–14513.
12. L. Schnitzspan, M. Kläui and G. Jakob, *Phys. Rev. Applied*, 2023, **20**, 024002.
13. P. Chureemart, R. F. L. Evans and R. W. Chantrell, *Phys. Rev. B*, 2011, **83**, 184416.
14. D.-H. Kim, D.-H. Kim, K.-J. Kim, K.-W. Moon, S. Yang, K.-J. Lee and S. K. Kim, *Journal of Magnetism and Magnetic Materials*, 2020, **514**, 167237.
15. C. Cai, Y. Wen, S. Liang, L. Yin, R. Cheng, H. Wang, X. Feng, L. Liu and J. He, *Nat. Commun.*, 2025, **16**, 10664.
16. M. Rodrigues, S. Basov, I. Madarevic, T. Saerbeck, M. Ferroni, P. Breckner, D. Isaia, L. Fulanović, A. Jafari, I. Sergueev, O. Leupold, M. J. Van Bael, A. Vantomme and K. Temst, *ACS Appl. Electron. Mater.*, 2024, **6**, 2289–2300.
17. B. Rana, *J. Appl. Phys.*, 2024, **136**, 150701.
18. S. Maity and S. Dwivedi, *Acta Mech. Sin.*, 2026, **42**, 424786.
19. Y.-M. Zhao, X.-W. Jin and Z.-Y. Yang, *New J. Phys.*, 2023, **25**, 113029.
20. B. B. Vermeulen, B. Sorée, S. Couet, K. Temst and V. D. Nguyen, *Micromachines*, 2024, **15**, 696.
21. S.-E. Park and T. R. Shrout, *J. Appl. Phys.*, 1997, 82, 1804–1811.
22. S. Y. Chen, H. Q. Zhang, Q. Y. Ye, Z. Q. Hu, Z. G. Huang and N. X. Sun, *J. Alloys Compd.*,

View Article Online
DOI: 10.1039/D6NA00074F

2016, **656**, 871–875.

23. D. Dagur, V. Polewczyk, A. Yu. Petrov, P. Carrara, M. Brioschi, S. Fiori, R. Cucini, G. Rossi, G. Panaccione, P. Torelli and G. Vinai, *Adv. Mater. Interfaces*, 2022, **9**, 2201337.
24. T. Wu, P. Zhao, M. Bao, A. Bur, J. L. Hockel, K. Wong, K. P. Mohanchandra, C. S. Lynch and G. P. Carman, *J. Appl. Phys.*, 2011, **109**, 124101.
25. E. Sun and W. Cao, *Progress in Materials Science*, 2014, **65**, 124–210.
26. Y. Yahagi, B. Harteneck, S. Cabrini and H. Schmidt, *Phys. Rev. B*, 2014, **90**, 140405.
27. Y. Zhang, W. Sun, K. Cao, X.-X. Yang, Y. Yang, S. Lu, A. Du, C. Hu, C. Feng, Y. Wang, J. Cai, B. Cui, H.-G. Piao, W. Zhao and Y. Zhao, *Sci. Adv.*, 2024, **10**, eadl4633.
28. Q. Li, A. Tan, A. Scholl, A. T. Young, M. Yang, C. Hwang, A. T. N'Diaye, E. Arenholz, J. Li and Z. Q. Qiu, *Appl. Phys. Lett.*, 2017, **110**, 262405.
29. R. Landauer, *IBM Journal of Research and Development*, 1961, **5**, 183–191.
30. X. Li, H. Singh, Y. Bao, Q. Luo, S. Li, J. Chatterjee, M. Goiriena-Goikoetxea, Z. Xiao, N. Tamura, R. N. Candler, L. You, J. Bokor and J. Hong, *Nano Lett.*, 2023, **23**, 6845–6851.
31. W. A. Misba, T. Kaisar, D. Bhattacharya and J. Atulasimha, *IEEE Trans. Electron Devices*, 2022, **69**, 1658–1666.
32. M. Hayashi, L. Thomas, R. Moriya, C. Rettner and S. S. P. Parkin, *Science*, 2008, **320**, 209–211.
33. K. Roy, *J. Phys. D: Appl. Phys.*, 2014, **47**, 422001.
34. S. Fukami, T. Suzuki, Y. Nakatani, N. Ishiwata, M. Yamanouchi, S. Ikeda, N. Kasai and H. Ohno, *Appl. Phys. Lett.*, 2011, **98**, 082504.

View Article Online
DOI: 10.1039/D6NA00074F

Data Availability Statement

The datasets supporting this article's findings are available from the corresponding author upon reasonable request. All raw data, micromagnetic simulation codes (OOMMF), and finite element analysis scripts (COMSOL) used in this study are archived in secure institutional repositories and can be provided to qualified researchers upon request. Additional materials, including high-resolution figure data and device fabrication parameters, are available upon request for replication or further analysis.